Modeling and Simulation of Surface-and-dive Behavior of a Bottlenose Dolphin

Usama Bin Sikandar[1], Abubakr Muhammad[1]

***Abstract*— In this paper, we present a biomechanical model capable of generating six-DoF trajectories of a swimming dolphin. Our model attempts to closely emulate an actual surfacing and diving dolphin. The degree of biomechanical complexity of our model stands as a reasonable compromise between a complicated flexible multi-link body and an overly-simplified point-mass. We constructed our model through analyzing previously reported results and statistics on hydrodynamics, kinematics, maneuverability and propulsive efficiency of bottlenose dolphins observed during their surface-and-dive, porpoising and foraging behaviors. The results of our model's computer simulations match the previous reports on the dolphins' buoyancy, depth profiles, and speeds during ascent, descent, and porpoising activities.**

I. Introduction

As inhabitants of a large part of temperate and tropical waters all over the world, bottlenose dolphins (*Tursiops truncatus*, *Tursiops aduncus* and *Tursiops australis*) emanate as the most extensively studied cetacean [1], [2]. Studies on their hydrodynamics, kinematics, maneuverability, behavior, power output and propulsive efficiency project their high performance swimming capabilities which progressively evolved and warranted their survival among a large number of competitive aquatic mammals and sharks. Moreover, research on the dolphin's cognition [3], migration [4], foraging strategies [5], [6], echolocation [7] and social behaviors [8] suggest that they socialize, particularly within their species, and cherish a reasonable level of intelligence.

We analyzed the results and statistics reported in some of these studies and, based on our analysis, constructed a vectorized six-DoF biomechanical model for the swimming dynamics of a dolphin. The degree of complexity of our biomechanical model stands as a reasonable compromise between a complicated flexible multi-link body and an overly-simplified point-mass. Although we assumed the dolphin body as rigid, we did incorporate body's moment of inertia; the roll, pitch and yaw torques; and the viscous torque. Additionally, considering the streamlined shape of the dolphin's body [9], the coefficient of viscous drag for transverse (sideways) motion had to be greater than the coefficient for longitudinal (forward) motion. We also modeled the change in buoyancy of the dolphin body as its inflated lungs collapse at greater depths [10]. So overall, we purposefully modeled the dolphin biomechanics in a way that avoids complex and long computations of real-time dolphin trajectories. In the end, we applied our model to simulate the surface-and-dive activity of a dolphin in 3D. Eventually, we plan to employ our simulator as a platform for testing vision- and biosonar-based dolphin-tracking techniques. Our simulation can also be employed to examine the physical phenomena that are hard to observe or measure.

[1]Authors are with Laboratory for Cyber Physical Networks and Systems (CYPHYNETS), Department of Electrical Engineering, Lahore University of Management Sciences (LUMS), Pakistan.

II. Methods

A. Overall Dynamic Model

1) Configuration Space: We modeled the dolphin's body as a rigid prolate spheroid [11], with l and w as lengths of major and minor axes respectively. The configuration of the dolphin can be specified in two coordinate frames: the world frame ${}^{\mathrm{W}}Oxyz$ and the body-attached frame (or body-frame) ${}^{\mathrm{B}}Oxyz$. In the world frame, the vector $\boldsymbol{x} = [x\ y\ z]^T$ represents position of the center of mass of the spheroid in 3D, and the vector $\boldsymbol{\theta} = [\psi\ \theta\ \phi]^T$ accumulates the variation in local roll, pitch and yaw angles of the spheroid. Hence, the overall configuration $\boldsymbol{q}(x, y, z, \psi, \theta, \phi)$ of the dolphin constitutes $\mathbb{R}^3 \times \mathbb{SO}(3)$. Vectors $\hat{\boldsymbol{r}}$ and $\hat{\boldsymbol{s}}$ in the world frame respectively represent dolphin model's head-direction $[1\ 0\ 0]^T$ and dorsal vector $[0\ 0\ 1]^T$ of the body frame. These vectors can be varied by applying a set of local roll, pitch and yaw rotations. After applying to $\hat{\boldsymbol{r}}$: first a roll of $\Delta\psi$ radians about the body x-axis, then a pitch of $\Delta\theta$ radians followed by a a yaw of $\Delta\phi$ radians about the body y- and z-axes respectively, we obtain the new head-direction

$$\hat{\boldsymbol{r}}_{\text{new}} = {}^{\mathrm{W}}_{\mathrm{B}}\mathbf{R}\ (\mathbf{R}_{x,\Delta\psi}\mathbf{R}_{y,\Delta\theta}\mathbf{R}_{z,\Delta\phi})\ {}^{\mathrm{B}}_{\mathrm{W}}\mathbf{R}\ \hat{\boldsymbol{r}}, \tag{1}$$

where the matrix ${}^{\mathrm{B}}_{\mathrm{W}}\mathbf{R}$ transforms $\hat{\boldsymbol{r}}$ from the world frame to the body frame [12].

2) Overview of the Modeling Technique: In this paper, we modeled the biomechanics of a dolphin body to simulate its surface-and-dive activity. As mammals, the dolphins cannot spend an extensive amount of time under water; they need to 'surface' (emerge out of the water surface for inspiration) regularly to cater for their body's oxygen requirements [9]. After surfacing, they dive back into the water and carry on their underwater activities with the new oxygen reserve. Our dolphin model emulates this behavior by ascending to the surface, diving back into the water, and then descending to a certain depth. These ascent and descent performances are driven by a particular path-plan whose phases are triggered by sensory information such as awareness of the current orientation, position, and speed of the model. A successful execution of the path-plan requires tracking the reference orientations ($\hat{\boldsymbol{r}}_{\text{ref}}$, $\hat{\boldsymbol{s}}_{\text{ref}}$) and reference speed ($v_{\text{ref}}$). As shown in the block diagram in Fig. 1, the translation and orientation controllers take $\hat{\boldsymbol{r}}_{\text{ref}}$, $\hat{\boldsymbol{s}}_{\text{ref}}$ and v_{ref} as inputs, and return appropriate thrust ($\boldsymbol{h}$) and torque ($\boldsymbol{\tau}$) vectors. The vector $\boldsymbol{h}$ (with magnitude h) acts as forcing function

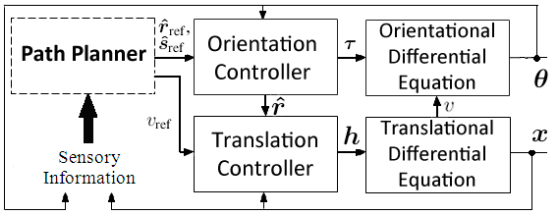

Fig. 1: The block diagram of the overall modeling technique.

of the nonlinear differential equation for translation, while $\boldsymbol{\tau}$ drives the nonlinear orientational differential equation. Solving these differential equations yields an overall six-DoF real-time trajectory of the dolphin model in $\boldsymbol{x}$ and $\boldsymbol{\theta}$.

B. Biomechanical Model

1) Translational Locomotion: While swimming, body of a dolphin experiences several forces such as gravity, drags, buoyant force, and self-generated thrust and lift. Equating the sum of all these external and internal forces to the net force on the body gives the translational differential equation of the system,

$$\mathbf{M}\ddot{\boldsymbol{x}} = \boldsymbol{f}_{\text{D}}(\dot{\boldsymbol{x}}, \boldsymbol{x}) + \boldsymbol{f}_{\text{B}}(\boldsymbol{x}) + \boldsymbol{h}(t), \tag{2}$$

where $\mathbf{M} = {}^{\text{W}}_{\text{B}}\mathbf{R}\ {}^{\text{B}}\mathbf{M}$, ${}^{\text{B}}M_{11} = {}^{\text{B}}M_{22} = {}^{\text{B}}M_{33} = m$, and ${}^{\text{B}}M_{ij} = 0$ for $i \neq j$, $\boldsymbol{f}_{\text{D}}$ is the drag force vector, $\boldsymbol{f}_{\text{B}}$ is the buoyancy vector (combined effect of the gravity and the buoyant force), and $\boldsymbol{h}$ is the sum of thrust and lift vectors which drive the differential equation and provide the propulsion required for swimming. For $\boldsymbol{f}_{\text{D}}$, we mathematically analyzed the speed-drag and speed-power relationships reported in the literature about experiments on gliding [10] and actively swimming dolphins [13], and constructed $\boldsymbol{f}_{\text{D}}$ as

$$\boldsymbol{f}_D(\dot{\boldsymbol{x}}, \boldsymbol{x}, t) = -\sigma(z)\gamma\Big(\frac{z}{w}\Big)||\dot{\boldsymbol{x}}||^2\ ({}^{\text{W}}_{\text{B}}\mathbf{R}\ \mathbf{C}(t)\ {}^{\text{B}}_{\text{W}}\mathbf{R})\ \hat{\dot{\boldsymbol{x}}}. \tag{3}$$

The sigmoid function $\sigma(z) = \frac{1}{\exp(\epsilon z)+1}$ (see Table I for numerical values of the modeling parameters) smoothly activates or inhibits the drag force across the boundaries of media (water and air, with water surface at $z = 0$). The function γ provides a drag-augmentation due to the influence of water surface [13], [14], [15], [16], and is given by

$$\gamma\Big(\frac{z}{w}\Big) = \begin{cases} 5 & \text{for } -\frac{z}{w} = 0.5, \\ \frac{8z}{5w} + \frac{29}{5} & \text{for } 0.5 < -\frac{z}{w} \leq 3, \\ 1 & \text{otherwise,} \end{cases}$$

where variation of γ in the mid-range $0.5 < -\frac{z}{w} \leq 3$ is assumed to maintain continuity with changing depth. The matrix $\mathbf{C}$ is a 3×3 tensor for coefficients of drag in the body frame, for which, $C(1,1) = 4.15\beta(t)$ for $h(t) = 0$ and $C(1,1) = 26.25$ otherwise, $C(2,2) = C(3,3) = \xi C(1,1)$, and $C(i,j) = 0$ for $i \neq j$. The function β increases the coefficient of drag against longitudinal motion, providing a braking mechanism. The parameter ξ raises the drag force against the transverse motion of the body. To calculate the transverse drag coefficient, we used a simplified model in which we assumed: the front of the dolphin as a flat circular plate with diameter w, and the side of its body as a flat elliptical plate with length l and width w. Using this simplification, the ratio between the longitudinal and transverse components of the drag turns out as the ratio of the surface areas of these elliptical and circular plates, resulting in $\xi = l/w$. The buoyancy vector, i.e. sum of buoyant force and weight vectors, is given by

$$\boldsymbol{f}_{\text{B}}(\boldsymbol{x}) = -\sigma(z)\rho_{\text{w}}V(z)\mathbf{g} + m\mathbf{g}, \tag{4}$$

where ρ_{w} is density of water, $\mathbf{g} = [0 \quad 0 \quad -9.81]^T$, and the volume V of the dolphin varies with a change in external pressure as the water depth varies. From [10],

$$V(z) = \begin{cases} \frac{V_{\text{lungs}}}{1-0.1z} + V_{\text{body}} & \text{for } z < 0, \\ V_{\text{lungs}} + V_{\text{body}} & \text{otherwise,} \end{cases} \tag{5}$$

where V_{lungs} is the volume of lungs at the atmospheric pressure, and V_{body} is the volume of a fully deflated body of a dolphin.

Dolphins have non-rigid elastic bodies allowing their flukes to oscillate dorsoventrally. Such fluke strokes produce a lift that is directed forward and upward during a downstroke, whereas forward and downward during an upstroke. The component of this lift directed towards the head-direction provides most of the forward thrust [13]. But for our purpose of tracking, we did not need to model the dolphin's body as elastic or multi-link. So to avoid unnecessary complications, we modeled the dolphin's body as rigid and finless. Consequently, the body of the model cannot oscillate its fluke to produce lift and forward propulsion. In our modeling technique, $\boldsymbol{h}$ is produced directly as an output of the thrust controller, and in turn, drives the translational differential equation. It can be represented as $\boldsymbol{h} = h_r\hat{\boldsymbol{r}} + h_s\hat{\boldsymbol{s}}$, where the components h_r and h_s provide forward propulsion and dorsal lift respectively.

2) Maneuverability: Defined as the animal's ability to turn in a confined space [17], maneuverability is measured in terms of body-length specific minimum turning radius (radius/length) and maximum turning rates, which are the indices of maneuverability in space and time respectively [5], [18], [19]. We will use the bounds on these indices of the foraging bottlenose dolphins as the bounds on our dolphin model's maneuverability because foraging dolphins need to exhibit a maximum maneuverability performance to compete with the superior maneuverability of their elusive prey [5], [19]. Dolphins can turn their bodies as well as perform complex barrel-roll maneuvers [20], performing rotations about the three orthogonal axes [9] of their bodies – incorporated in our model as local roll, pitch and yaw. Dolphins can employ drag- and lift-based maneuverability mechanisms [13] that provide torque and centripetal force for body rotation and turning. Because we modeled the dolphin body as rigid and fin-less, we generate the torque $\boldsymbol{\tau}$ directly from our maneuverability (or orientation) controller. Equating the net torque on the body to the sum of $\boldsymbol{\tau}$ and the viscous torque $\boldsymbol{\tau}_{\text{D}}$ leads to the differential equation

$$\boldsymbol{\Lambda}\ddot{\boldsymbol{\theta}} = \boldsymbol{\tau}_{\text{D}}(\dot{\boldsymbol{\theta}}) + \boldsymbol{\tau}(t), \tag{6}$$

where $\boldsymbol{\Lambda}$ is the moment of inertia tensor for a prolate spheroid with the axes of rotation passing through its center

of mass; $\Lambda_{11} = \frac{2}{5}mw^2$, $\Lambda_{22} = \Lambda_{33} = \frac{1}{5}m(l^2 + w^2)$, and $\Lambda_{ij} = 0$ for $i \neq j$ [21]. The vector $\boldsymbol{\tau}$ drives the differential equation and is computed from the maneuverability controller described in section II-C.2. As an additional remark, we did not directly couple (6) and (2) to avoid any futile complications between maneuverability and translation.

C. Control

A certain speed of the dolphin model is maintained through an appropriate h, the output of the thrust controller. The orientation is controlled by tracking reference $\hat{\boldsymbol{r}}$ and $\hat{\boldsymbol{s}}$ through a controller that returns $\boldsymbol{\tau}$. These controllers may not reflect the dolphin's actual motor controls; they just serve as adequate surrogates to emulate reference tracking.

1) Thrust Control: Dolphins have been observed to maintain constant speeds under water, specific to certain activities [9], [10], [22]. To model such a regulation, we implemented a control for achieving a reference speed v_{ref}. From Newton's Second Law of motion, the magnitude of the thrust vector $h = ma_{\text{out}}$. The output a_{out} of the controller at a particular time instance represents the model's target acceleration, and is calculated as the output of the PID controller with parameters k_p, k_i and k_d. But a_{out} can become unbounded. So, we determined the numerical value of maximum dolphin acceleration from [23], and we could not find in the literature any evidence for their backwards thrust generation. Hence, we limited a_{out} in the range $0 \leq a_{\text{out}} \leq a_{\max}$. Then building upon our modeling strategy as discussed at the end of section II-B.1, we ignored the transverse component $h_s\hat{\boldsymbol{s}}$ of $\boldsymbol{h}$ because we can generate the desired dolphin trajectories without it. Therefore, $\boldsymbol{h} = h\hat{\boldsymbol{r}}$, the forcing function of the differential equation (2).

At greater depths, the dolphin model may lose control over its speed due to smaller buoyant force acting against the gravity. To avoid similar loss of control, dolphins apply different braking mechanisms such as raising their flukes or extending their appendages [9]. Using a drag augmentation factor of 11.5 observed by Skrovan et al. when a dolphin raised its fluke [10], the braking coefficient β can be implemented as a sigmoid function of time, given by

$$\beta(t, t_0) = \begin{cases} \frac{23}{\exp\left(-\zeta(t-t_0)\right)+1} - 11.5 & \text{for } \dot{e} > 0,\ t \geq t_0, \\ 1 & \text{otherwise,} \end{cases} \tag{7}$$

where ζ is the activation rate, t_0 is the time instance when brakes are applied, and $e = v_{\text{ref}} - v$.

2) Maneuverability Control: To cause a change in the orientation $\boldsymbol{\theta}$ of the model, we need a controller that takes a reference $\boldsymbol{\theta}_{\text{ref}}$ as input, and returns the torque $\boldsymbol{\tau}$ required to track the reference, where $\boldsymbol{\theta}_{\text{ref}} = [\Delta\psi_{\text{ref}} \ \ \Delta\theta_{\text{ref}} \ \ \Delta\phi_{\text{ref}}]^T$. We devised a technique to calculate $\boldsymbol{\theta}_{\text{ref}}$ for tracking a reference orientation of the model, specified by $\hat{\boldsymbol{r}}_{\text{ref}}$ and $\hat{\boldsymbol{s}}_{\text{ref}}$. To head in a new direction, the dolphin model must orient its head-direction towards $\hat{\boldsymbol{r}}_{\text{ref}}$, which may be available directly from a path-plan. For the case where the model needs to track a target at a point with position vector $\boldsymbol{p}$ in the world frame, $\hat{\boldsymbol{r}}_{\text{ref}}$ can be calculated from $\hat{\boldsymbol{r}}_{\text{ref}} = \boldsymbol{p} - \boldsymbol{x}$. This means that in the body-frame, ${}^{\text{B}}\hat{\boldsymbol{r}}$ must align with the vector ${}^{\text{B}}\hat{\boldsymbol{r}}_{\text{ref}}$ given by the vector ${}^{\text{B}}\boldsymbol{u} = {}^{\text{B}}_{\text{W}}\mathbf{R}\hat{\boldsymbol{r}}_{\text{ref}}$. Now to align ${}^{\text{B}}\hat{\boldsymbol{r}}$ with ${}^{\text{B}}\boldsymbol{u}$, the required changes in the angles of elevation and azimuth must be calculated, which are the local pitch $\Delta\theta_{\text{ref}}$ and local yaw $\Delta\phi_{\text{ref}}$ rotations respectively, calculated as $\Delta\theta_{\text{ref}} = -\tan^{-1}\left({}^{\text{B}}u_z/\sqrt{({}^{\text{B}}u_x)^2 + ({}^{\text{B}}u_y)^2}\ \right)$, and $\Delta\phi_{\text{ref}} = \tan^{-1}({}^{\text{B}}u_y/{}^{\text{B}}u_x)$. For $\Delta\psi_{\text{ref}}$ component, we need to first decide a criterion for setting a reference $\hat{\boldsymbol{s}}$ direction. In the literature, we could not find any evidence of upside down swimming of the bottlenose dolphins. So for our model, such an orientation can be avoided by ensuring that the inner product of $\hat{\boldsymbol{s}}$ and positive z-direction is never negative. This can be implemented just through appropriate roll maneuvers. Now with $\hat{\boldsymbol{s}}_{\text{ref}} = [0\ 0\ 1]^T$, a new ${}^{\text{B}}\boldsymbol{u}$ is calculated. But only the roll component of the required overall maneuver is picked and placed as $\Delta\psi_{\text{ref}} = -\tan^{-1}({}^{\text{B}}u_y/{}^{\text{B}}u_z)$.

The maneuverability controller takes $\boldsymbol{\theta}_{\text{ref}}$ as input, and returns a torque pseudo-vector $\boldsymbol{\tau}$. Choosing $\boldsymbol{\tau} = \boldsymbol{\Lambda}\ddot{\boldsymbol{\theta}}_{\text{out}}$, and applying feedback linearization with $\ddot{\boldsymbol{\theta}}_{\text{out}} = \boldsymbol{\Lambda}^{-1}(\boldsymbol{\tau}_{\text{D}} + \boldsymbol{\mu})$, (6) reduces to $\ddot{\boldsymbol{\theta}} = \boldsymbol{\mu}$, where the vector $\boldsymbol{\mu}$ represents the output of a PID controller with parameter matrices $\mathbf{K}_p$, $\mathbf{K}_i$ and $\mathbf{K}_d$, and input vector $\boldsymbol{\varepsilon} = \boldsymbol{\theta}_{\text{ref}} - \boldsymbol{\theta}$. It has been reported previously that the turning force on a dolphin's body is directly proportional to the square of its linear speed [18]. Hence, in our model, we modify the pitch and yaw components of $\boldsymbol{\mu}$ (μ_θ and μ_ϕ) by multiplying them with v^2 because pitch and yaw displacements combine to produce an overall turning. While turning towards a reference orientation as well as swimming at a non-zero speed, the model will follow a curved path. Realistically, the angular speed for turning along such a curve must be bounded, which is corroborated by the past research on maneuverability of dolphins [5]. This can be ensured through applying appropriate bounds on $\boldsymbol{\tau}$. Let the bounds on the angular speeds be $\dot{\psi}_{\max}$ for rolling and $\omega_{\max}$ for turning. Rolling and turning at these bounds on angular speed indicate that the generated torque adequately counters the viscous torque experienced at these bounds. So, we specified the thresholds on rolling and turning components of $\boldsymbol{\tau}$ as magnitudes of viscous torques against rolling and turning at $\dot{\psi}_{\max}$ and $\omega_{\max}$ respectively.

Eventually, the outputs from the thrust and maneuverability controllers drive the differential equations (2) and (6) respectively.

D. Swimming Behavior Model

The swimming behavior of dolphins is adapted to maximize their locomotor efficiency [24]. They switch between stroking and gliding to optimize their locomotor costs, classified as burst-and-glide (or burst-and-coast) mode of swimming [10], [23], [25]. In this mode, a dolphin achieves the speed $v_{\max}$ through rapid stroking (burst) and then glides (or coasts) for some time until decelerating down to the speed $v_{\min}$. It carries on stroking and gliding in this fashion to minimize the locomotion costs. Our model exhibits the burst-and-glide mode of swimming through alternatingly tracking $v_{\min}$ and $v_{\max}$. If the speed of the dolphin model nears $v_{\min}$, it starts active swimming with thrust magnitude $h > 0$. But as soon as the speed rises to $v_{\max}$, h is set to zero so that

the model glides and decelerates down to v_{min} through the effect of incorporated drags.

1) Surface-and-dive Activity: As a mammal, 'surfacing' (approaching the water surface for inspiration) is vital for a dolphin. Based on the observations reported in [10] and [23], we divided the whole surfacing event into four phases. In phase 1, if the dolphin model is below the water surface, it orients its head-direction $\hat{\boldsymbol{r}}$ towards the world positive z-axis, and ascends towards the surface in a burst-and-glide mode (v^a_{min}, v^a_{max}). On rising up to a depth z_1, phase 2 begins in which the model's reference orientation is set so that the body emerges out of the water at an angle α_1, and the reference speed is set to zero to cause a deceleration that prevents the model from leaping too high into the air. When the model rises to a depth z_2 just before emerging out, phase 3 begins and it starts adjusting its body for a dive back into the water. After leaping back in, depth z_3 marks the beginning of the fourth phase in which the world frame's negative z-axis is set as the reference orientation. Now, the descent begins and the model swims in a burst-and-glide fashion (v^d_{min}, v^d_{max}).

2) Porpoising: We simulated the porpoising activity as an application of the surface-and-dive modeling. According to our porpoising model, which is partly inspired from the research in [23], it is a four-phase activity. As the first phase begins, the dolphin model swims actively near and parallel to the water surface, just below a depth z_p. On achieving the reference speed v_f, phase 2 begins and the model orients itself to leap out, making an angle α_1 with the water surface. After leaping out, phase 3 begins in which the models orients to leap back into the water, at an angle α_2. The reference speed is now set to v_i, which is less than v_f because the model should now glide to slow down. As soon as the model gets below z_p, phase 4 begins and the model orients itself parallel to the water surface and continues gliding. When the speed slows down to v_i, phase 1 begins again. In this way, the dolphin model carries on porpoising periodically.

III. Results

Using the values of the modeling parameters given in Table I, we simulated our biomechanic model in Matlab by numerically solving the differential equations (2) and (6) through Euler's approximation. The solutions of these equations are trajectories in $\boldsymbol{x}(t)$ and $\boldsymbol{\theta}(t)$ respectively. Computing one hour of real-time simulation through our code in Matlab took roughly 15 minutes.

A. Buoyancy

The dolphin model experiences an upward force beneath the water surface above a depth of roughly 16 m, and a downward force below this depth. This is a consequence of modeling by (5) the changing body-volume with changing depth, as proposed by Skrovan et al. [10]. They observed that a 177 kg dolphin experienced net buoyancy of $+21.0$ N at 5.5 m depth and -22.1 N at a depth of 67.5 m. Our modeling technique based on their proposition resulted in a net buoyancy of $+24.3$ N at 5.5 m and -25.7 N at 67.5 m – for a 170.9 kg model with a lung volume of 0.00851 m^3.

TABLE I: Numerical values of the modeling parameters. Values were assumed that could not be found in the literature.

Parameter	Value	Reference
l, w, ξ	2, 0.4, 5	
V_{lungs}, V_{body}	0.00851, 0.1676	[10]
ρ_{w}, ρ_{d} (body density)	1000, 1020	
$m = \frac{1}{6}\pi\rho_d l w^2$	170.9	
a_{max}, $\dot{\psi}_{\text{max}}$, ω_{max}	6.54, 6.28, 23.95	[23], [5]
(v^a_{min} v^a_{max}), (v^d_{min} v^d_{max})	(1.2 1.9), (1.8 2.2)	[10]
v_i, v_f	$4.92, 6.56$	[23]
ϵ, ζ	$160, 2$	
k_p, k_i, k_d	80, 0.01, 0	
$\mathbf{K}_d, \mathbf{K}_p$, $\mathbf{K}_i$	$40\mathbf{I}$, $0.25\mathbf{K}_d^2$, $\mathbf{0}$	
z_1, z_2, z_3, z_p	$-1, -0.2, -1, -2$	
α_1, α_2	$39^\circ, 39^\circ$	[23]

B. Ascent and Descent

Fig. 2 shows the 3D spatial plot of an ascent, followed by surfacing and a descent to roughly 25 m. Variation in speed of the dolphin model for this trajectory is shown Fig. 3a. Fig. 3b shows the cumulative roll, pitch and yaw displacements over time, plotted along the tracking errors. We can observe that the controllers successfully track the references, and the tracking errors decay to zero.

Fig. 4a shows the depth profile and speed variation of the dolphin model for a deep descent followed by an immediate ascent in a single trajectory. Graph A shows that the dolphin model descends down to a depth of below 100 m and immediately begins to ascend towards the surface for inspiration, whereas graph B shows the speed variation in this trajectory. These graphs can be compared to the plots shown in Fig. 4b which depict an actual trajectory of a dolphin as reported in [10]. We can observe that after the descent, the dolphin stations for roughly 20 s below 110 m and then begins its ascent for surfacing. In our simulated trajectory, modeling the descent swimming mode as burst-and-glide causes the speed of the dolphin model to vary between 1.2 and 1.9 ms^{-1}. In the simulation, we observed that even if the model glides down below 60 m within these limits, the absence of a braking mechanism causes its speed to increase indefinitely – indicating a loss of control over the speed. This is the consequence of dolphin's weight overwhelming its body's buoyancy. So, between 40 and 80 s, the dolphin model needed to brake slightly to decelerate down to the speed of 1.2 ms^{-1}. Similar deceleration variation can be seen for the actual dolphin in the graph B of Fig. 4b. But in [10], researchers reported that the dolphin glided during this interval; they may have overlooked its attempts at braking. At the end of descent at about 80 s in Fig. 4a graph A, the dolphin model needed to reorient itself to start ascending. So, it decelerated sharply to a speed below 0.5 ms^{-1}, preventing itself from descending any further. This sharp deceleration is similar to the deceleration exhibited by the real dolphin in Fig. 4b graph A near 80 s, after which it stationed for about 20 s before accelerating rapidly to a speed of 2 ms^{-1}. At this point, the dolphin began to ascend with its speed oscillating about 2 ms^{-1}. Fig. 4a shows that our model also applied a rapid acceleration at the start of ascent

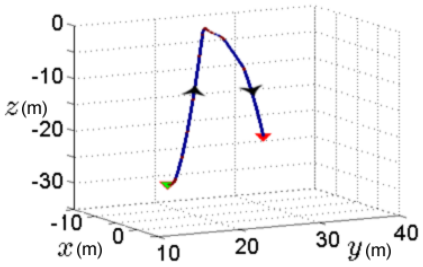

Fig. 2: The 3D trajectory of an ascent, a surfacing event, and a subsequent descent of the dolphin model.

and then varied its speed about 2 ms^{-1} while ascending. Our modeled speed variation is more rapid because we did not incorporate different stroking modes such as small- and medium-amplitude strokes – usually employed to generate small accelerations or to maintain smaller speeds [10].

C. Porpoising

Fig. 5a shows the spatial plot of a porpoising leap that we simulated, while Fig. 5b shows the variation in speed during this leap. Referring to the three-phase model of porpoising proposed in [23], at point A phase 1 begins where the model starts stroking to accelerate up to a speed close to 7 ms^{-1}. Although it continuously strokes while moving from A to B, the augmented drag near the water surface counters the thrust and initially makes the model decelerate. But just before leaping, the thrust wins over and causes the model to leap out at a speed of roughly 6.6 ms^{-1}. Then phase 2 begins, and the conservation between gravitational potential and kinetic energies makes the model return to the water surface at C with the same speed that was at B [23]. Leaping back into the water marks the beginning of phase 3 in which the model glides and decelerates to below 5 ms^{-1}. It has been observed that the leaps are interspersed by relatively long swimming bouts, represented by sections CA and AB, about twice the leap length [23]. From our data of 250 simulated leaps, the average ratio of a horizontal distance covered under the water surface between two leaps, to the leap length, was calculated

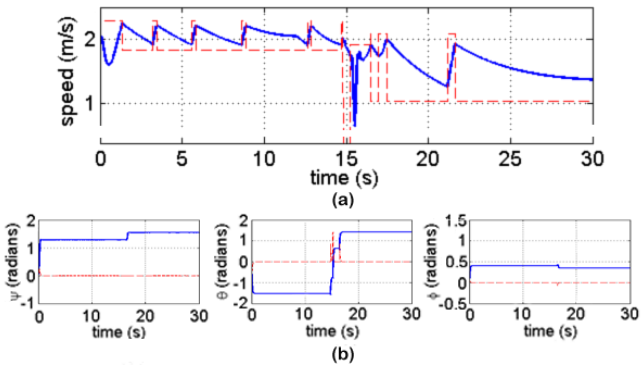

Fig. 3: (a) Variation in speed of the dolphin model for trajectory shown in Fig. 2. Dashed-line plot in red shows the reference speed. (b) Variation in accumulating roll, pitch and yaw displacements of the dolphin model for trajectory shown in Fig. 2. Dashed-line plots in red represent tracking errors.

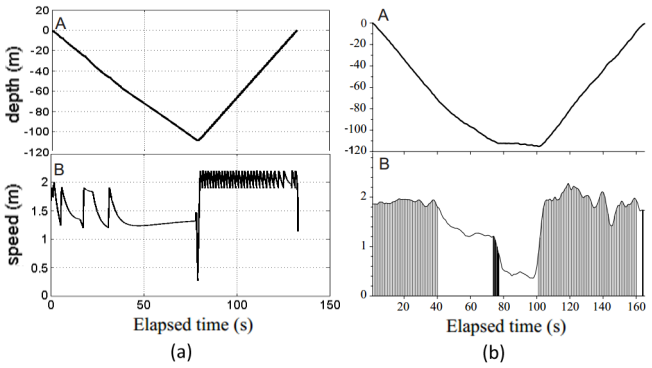

Fig. 4: (a) Graphs for a simulated trajectory of the dolphin model, depicting variation in depth (A) and speed (B) for a descent and a subsequent ascent. (b) Graphs for a real dolphin trajectory as reported by Skrovan et al. [10], depicting variation in depth (A) and speed (B) for a descent and a subsequent ascent.

as 2.7; close to the approximate factor of 2.

IV. Discussion

In this paper, we presented a biomechanical model of a bottlenose dolphin, assuming the body of the dolphin as a rigid spheroid, and simulated its surface-and-dive and porpoising activities. The model for translation incorporates the three-dimensional viscous drag acting on the dolphin's body. Many researchers have tried to deduce a relationship between drag force and linear speed of a dolphin's body. Skrovan et al. [10] has reported the relationship between drag force's magnitude f_{D} and speed v of a gliding dolphin as $f_{\text{D}} = 4.15v^2$. But for an actively swimming dolphin, we derived (see Appendix I) the drag-speed relationship as $f_{\text{D}} = 26.25v^2$, which is based on Fish's least-square regression equation [13].

Maresh et al. observed the dolphins' ability to turn with a maximum turning rate of 1372.0°s^{-1} (23.946 rads^{-1}) [5]. This turning rate ω is defined about the center of the turning circle. However, we turn our model by rotating its body about its center of mass with turning rates $\dot{\theta}$ (for pitch) and $\dot{\phi}$ (for yaw) at a non-zero speed. So we must establish a mapping

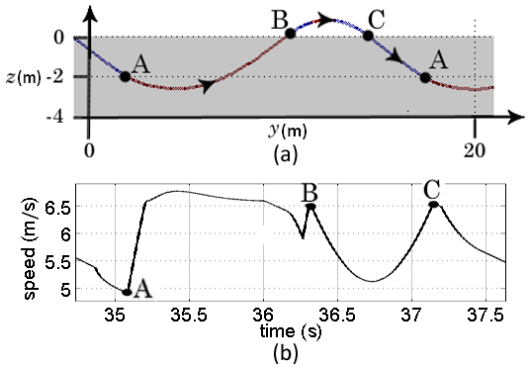

Fig. 5: (a) Trajectory of a porpoising dolphin model leaping in the y-z plane. Line $z = 0$ represents the water-air boundary. (b) Variation in speed of the leaping dolphin model shown in (a).

between ω and $\dot{\theta}$ (and $\dot{\phi}$). For a range of realistic [5], [9] magnitudes of thrusts (h) and turning rates ($\dot{\theta}$), we computed the maximum percentage difference between ω and $\dot{\theta}$, at constant speeds as 0.53% – which is insignificant. Therefore, for planar turns we can assume that $\omega = \dot{\theta}$. In 3D, both pitch and yaw rotations cause an overall turning of the model's body, implying that ω must equal an overall angular speed in pitch and yaw. But for small linear speeds close to zero, ω may not be equal to $\dot{\theta}$ because a large torque can rotate the body about its center of mass without making it execute a turn. So to compensate for it, we set the turning force as directly proportional to the square of the linear velocity, which is indeed a real phenomenon [18].

In order to change the thrust magnitude, dolphins vary their swim-stroke amplitudes. To accelerate up to a certain speed, the amplitude may transition from large to medium, and eventually die down to small values [10], indicating a gradual decrease in the applied thrust until achieving the target speed. During the ascent stage of a deep dive, dolphins need to counter the gravity through a higher thrust. Hence, to accelerate or to maintain a certain speed, they need to stroke at high or medium amplitude for much longer distances as compared to the descent stage. In our model, we did not incorporate the effects of varying magnitudes of stroking. This results in a burst of large thrust at the beginning of an acceleration, representing a large amplitude thrust. Moreover, because medium-amplitude stroking is not used to maintain a certain speed, the percentage time spent in active swimming during ascent stages of our simulation was different from that reported by Skrovan et al. [10].

V. Conclusions and Future Work

In this paper, we presented a compromised model for the biomechanics of a bottlenose dolphin, assuming its body as a rigid spheroid, and simulated the surface-and-dive and the porpoising activities. In future, we will incorporate in our model the dolphin's bioacoustics and other behaviors (migration, prey-search and foraging etc.). We plan to implement these behaviors through behavior-based modeling and control.

Acknowledgments

We would like to express our gratitude to WWF-Pakistan for their financial support in this project.

APPENDIX I: Calculations

Fish reports a least square regression as $P = 28.87v^{2.91}$ [13], between a speed v of an actively swimming dolphin and the thrust power P required to maintain that v. This power is the rate of work done by the dolphin against the drag force f_{D} that points exactly opposite to the direction of speed and does not vary at constant v. Hence, from the relationship $P = f_{\mathrm{D}}v$, we can deduce that $f_{\mathrm{D}} = 28.87v^{1.91}$. For simplicity, we rounded up the exponent of v to 2 and compensated for it by decreasing the coefficient by a factor of 1.1 ($\frac{v^2}{v^{1.91}} = v^{0.09} \simeq 1.1$ at average dolphin swimming speeds [22]). Finally, $f_{\mathrm{D}} = 26.25v^2$.

References

[1] H. Shirihai, and B. Jarrett, "Whales Dolphins and Other Marine Mammals of the World." Princeton: Princeton Univ. Press, 2006, pp. 159–161.

[2] K. Charlton-Robb, L. Gershwin, R. Thompson, J. Austin, and K. Owen et al., "A New Dolphin Species, the Burrunan Dolphin *Tursiops australis* sp. nov., Endemic to Southern Australian Coastal Waters" PLoS ONE (Public Library of Sci.), vol. 6, no. 9, pp. e24047, 2011.

[3] R. Schusterman, J. Thomas, and F. Wood. "Dolphin Cognition and Behavior: A Comparative Approach." Lawrence Erlbaum associates, Publishers, Hillsdale, NJ, 1986.

[4] E. L. Estrada, and A. A. Hohn. "Satellite monitored movements of bottlenose dolphins along the Atlantic coast of the US." 15th Biennial Conference on the Biology of Marine Mammals, Greensboro, North Carolina, 14-19 December 2003.

[5] J. L. Maresh, F. E. Fish, D. P. Nowacek, and S. M. Nowacek. "High Performance Swimming Capabilities During Foraging by Bottlenose Dolphins (*Tursiops truncatus*)." Marine Mammal Sci., vol. 20, no. 3, pp. 498–504, 2004.

[6] T. M. Willaims, "Strategies for reducing foraging costs in dolphins. In Aquatic Predators and their Prey." (ed. S. P. R. Greenstreet and M. L. Tasker). Cambridge: Blackwell Scientific Publications, Oxford, 1996, pp. 4–9.

[7] W. W. L. Au. "The SONAR of Dolphins." New York: Springer-Verlag, 1993.

[8] D. P. Nowacek. "Sound Use, Sequential Behavior and Ecology of Foraging Bottlenose Dolphins, *Tursiops truncatus*." Doctoral Dissertation, Woods Hole Ocean. Inst., MIT, CA, MA, 1999.

[9] F. E. Fish, and J. J. Rohr. "Review of Dolphin Hydrodynamics and Performance." SSC San Diego, 1999.

[10] R. C. Skrovan, T. M. Williams, P. S. Berry, P. W. Moore, and R. W. Davis. "The diving physiology of bottlenose dolphins (*Tursiops truncatus*). II. Biomechanics and changes in buoyancy at depth." J. Exp. Biol., vol. 202, pp. 2749–2761, 1999.

[11] D. Weihs. "The Hydrodynamics of Dolphin Drafting." J. Biol., vol. 3, no. 2, pp. 8.1–8.16, 2004.

[12] M. W. Spong, and M. Vidyasagar. "Robot Dynamics and Control." Wiley, 1989.

[13] F. E. Fish. "Power output and propulsive efficiency of swimming bottlenose dolphins (*Tursiops truncatus*)." J. Exp. Biol., vol. 185, pp. 179–193, 1993.

[14] H. Hertel. "Hydrodynamics of Wave-riding Dolphins." In *The Biol. of Marine Mammals*, H. T. Andersen, Ed. Academic Press, New York, NY, 1969, pp. 31–63.

[15] R. W. Blake. "Energetics of Leaping in Dolphins and Other Aquatic Animals" J. Mar. Biol. Ass. U.K., vol. 63, pp. 61–70, 1983.

[16] D. Au, and D. Weihs. "At high speeds dolphins save energy by leaping." Nature, vol. 284, no. 5756, pp. 548–550, 1980.

[17] U. Norberg, and J. M. V. Rayner. "Ecological Morphology and flight in bats (Mammalia: Chiroptera): Wing adaptation, flight performance, foraging strategy and echolocation." Philosph. Trans. of the Roy. Soc. B, vol. 316, pp. 335–427, 1987.

[18] H. C. Howland. "Optimal Strategies for Predator Avoidance: The Relative Importance of Speed and Manoeuvrability." J. Theor. Biol., vol. 47, pp. 333–350, 1974.

[19] P. Domenici, and R. W. Blake. "The Kinematics and Performance of the Escape Responce in the Angelfish (*Pterophyllum eimekei*)." J. Exp. Biol., vol. 156, pp. 187–205, 1991

[20] L. Marino, and J. Stowe. "Lateralized Behavior in Two Captive Bottlenose Dolphins (*Tursiops truncatus*)." Zoo. Biol., vol. 16, pp. 173–177, 1997.

[21] H. G. Goldstein. "Classical Mechanics" (2nd ed.), Addison Wesley, 1980, ch. 5.

[22] C. Lockyer, and R. Morris. "Observations on diving behavior and swimming speeds in a wild juvenile *Tursiops truncatus*." Aquatic Mammals, vol. 13, no. 1, pp. 31–35, 1987.

[23] D. Weihs. "Dynamics of Dolphin Porpoising Revisited." Integr. Comp. Biol., vol. 42, pp. 1071–1078, 2002.

[24] T. M. Willaims, W. A. Friedl, J. E. Haun, and N. K. Chun. "Balancing power and speed in bottlenose dolphins (*Tursiops truncatus*)." In Marine Mammals: Advances in Behavioural and Population Biol., vol. 66, ed. I. L. Boyd, Oxford: Clarendon Press, 1993, pp. 383–394.

[25] D. Weihs. "Energetic advantages of burst swimming of fish." J. Theor. Biol., vol. 48, pp. 215–229, 1974.